Rapid high resolution imaging of diffusive properties in turbid media

Frank Scheffold[1,*] **and Ian D. Block**[1,2]

[1]*Department of Physics and Fribourg Center for Nanomaterials, University of Fribourg, 1700 Fribourg, Switzerland*

[2]*LS Instruments AG, Rte St-Nicolas-de-Fle, 1700 Fribourg, Switzerland*

[*]*frank.scheffold@unifr.ch*

http://physics.unifr.ch/en/page/54/

http://www.lsinstruments.ch/

Abstract: We propose a laser speckle based scheme that allows the analysis of local scattering properties of light diffusely reflected from turbid media. This turbid medium can be a soft material such as a colloidal or polymeric material but can also be biological tissue. The method provides a 2D map of the scattering properties of a complex, multiple scattering medium by recording a single image. We demonstrate that the measured speckle contrast can be directly related to the local transport mean free path l^* or the reduced scattering coefficient $\mu_t = 1/l^*$ of the medium. In comparison to some other approaches, the method does not require scanning (of a laser beam, detector or the sample itself) in order to generate a spatial map. It can conveniently be applied in a reflection geometry and provides a single characteristic value at any given position with an intrinsic resolution typically on the order of 5-50 μm. The actual resolution is however limited by the transport mean free path itself and can thus range from microns to millimeters.

OCIS codes: (030.6140) Speckle; (110.6150) Speckle imaging; (170.3880) Medical and biological imaging.

References and links

1. E. Paruta-Tuarez, H. Fersadou, V. Sadder, P. Marchal, L. Choplin, C. Baravian, and C. Castel, "Highly concentrated emulsions: 1. average drop size determination by analysis of incoherent polarized steady light transport," J. Colloid Interface Sci. **346**(1), 136–142 (2010).
2. C. Baravian, F. Caton, J. Dillet, and J. Mougel, "Steady light transport under flow: characterization of evolving dense random media," Phys. Rev. E **71,** 066603 (2005).
3. H. M. Wyss, S. Romer, F. Scheffold, P. Schurtenberger, and L. J. Gauckler, "Diffusing-wave spectroscopy of concentrated alumina suspensions during gelation," J. Colloid Interface Sci. **240,** 89–97 (2001).
4. P. Snabre, L. Brunel, and G. Meunier, "Multiple light scattering methods for dispersion characterization and control of particulate processes," in *Particle Sizing and Characterization*, ed. T. Provder and J. Texter, (American Chemical Society, Washington DC, 2004).
5. F ormulaction SA (Bordeaux, France) web: http://www.formulaction.com/, LSInstruments AG (Fribourg, Switzerland) web: http://www.lsinstruments.ch.
6. A. Yodh and B. Chance, "Spectroscopy and imaging with diffuse light," Phys. Today **48**(3), 34–40 (1995).
7. F. Bevilacqua, D. Piguet, P. Marquet, J. Gross, B. Tromberg, and C. Depeursinge, "In vivo local determination of tissue optical properties: applications to human brain," Appl. Opt. **38**(22), 4939–4950.

#155084 - $15.00 USD Received 20 Sep 2011; revised 24 Nov 2011; accepted 28 Nov 2011; published 20 Dec 2011

8. R. B. Schulz, J. Ripoll, and V. Ntziachristos, "Noncontact optical tomography of turbid media," Opt. Lett. **28,** 1701–1703 (2003).
9. D. A. Weitz and D. J. Pine, "Diffusing wave spectrscopy," in *Dynamic Light Scattering*, ed. W. Brown, (Oxford University Press, 1992).
10. P. D. Kaplan, A. D. Dinsmore and A. G. Yodh, "Diffuse-transmission spectroscopy: A structural probe of opaque colloidal mixtures," Phys. Rev. E **50**, 4827–4835 (1994).
11. C. Aegerter and G. Maret, "Coherent backscattering and anderson localization of light," Prog. Opt. **52**, 1–62 (2009).
12. D. Cuccia, F. Bevilacqua, A. J. Durkin, F. Ayers, and B. Tromberg, "Quantitation and mapping of tissue optical properties using modulated imaging," J. Biomed. Opt. **14**(2), 024012 (2009).
13. A. Joshi, W. Bangerth, and E. M. Sevick-Muraca, "Non-contact fluorescence optical tomography with scanning patterned illumination," Opt. Express **14**, 6516–6534 (2006).
14. J. W. Goodman, *Speckle Phenomena in Optics* (Roberts & Company, 2007).
15. D. Magatti, A. Gatti and F. Ferri, "Three dimensional coherence of light speckles: experiment," Phys. Rev. A **79**, 053831 (2009).
16. S. E. Skipetrov, J. Peuser, R. Cerbino, P. Zakharov, B. Weber, and F. Scheffold, "Noise in laser speckle correlation and imaging techniques," Opt. Express **18**, 14519–14534 (2010).
17. M. Erpelding, A. Amon, and J. E. Crassous, "Diffusive wave spectroscopy applied to the spatially resolved deformation of a solid," Phys. Rev. E **78**, 046104 (2008).
18. P. Zakharov and F. Scheffold, "Monitoring spatially heterogeneous dynamics in a drying colloidal thin film," Soft Mater. **8**, 102–113 (2010).
19. L. F. Rojas-Ochoa, S. Romer, F. Scheffold, and P. Schurtenberger, "Diffusing wave spectroscopy and small-angle neutron scattering from concentrated colloidal suspensions," Phys. Rev. E **65**, 051403 (2002), [http://www.lsinstruments.ch/scattering_calculator/].
20. J. Peuser, A. Belhaj-Saif, A. Hamadjida, E. Schmidlin, A. D. Gindrat, A. C. Völker, P. Zakharov, H. M. Hoogewoud, E. M. Rouiller and F. Scheffold, "Follow-up of cortical activity and structure after lesion with laser speckle imaging and magnetic resonance imaging in nonhuman primates," J. Biomed. Opt. **16**, 096011 (2011).
21. P. Zakharov, A. Völker, A. Buck, B. Weber, and F. Scheffold, "Quantitative modeling of laser speckle imaging," Opt. Lett. **31** (23), 3465 (2006).
22. N. Curry, P. Bondareff, M. Leclercy, N. F. van Hulst, R. Sapienza, S. Gigan, and S. Gresillon, "Direct determination of diffusion properties of random media from speckle contrast," Opt. Lett. **36**(17), 3332–3334 (2011).
23. O. L. Muskens and A. Lagendijk, "Broadband enhanced backscattering spectroscopy of strongly scattering media," Opt. Express **16**(2), 1222 (2008).
24. J. C. Ragain Jr. and W. M. Johnston, "Accuracy of Kubelka-Munk reflectance theory applied to human dentin and enamel," J. Dent. Res. **80**, 449 (2001).
25. B. Weber, C. Burger, M. T. Wyss, G. K. von Schulthess, F. Scheffold, and A. Buck. "Optical imaging of the spatiotemporal dynamics of cerebral blood flow and oxidative metabolism in the rat barrel cortex," Eur. J. Neurosci. **20**(10), 2664 (2004).

1. Introduction

The determination of a sample's optical scattering properties is important for a diverse set of fundamental research areas and industrial applications ranging from stability monitoring of complex fluids and formulations (for example to differentiate sedimentation, creaming, phase separation) [1–3] to *in-vivo* biological studies of tissue composition and blood perfusion [4–8]. A number of techniques exist which provide a single measurement of the scattering properties of a given sample volume. Diffusing Wave Spectroscopy (DWS) [9] (or "Diffuse Transmission Spectroscopy" [10]) and coherent backscattering [11] are such techniques that can measure the scattering strength of a diffusive medium through determination of a characteristic parameter known as the transport mean free path l^* or the reduced scattering coefficient $\mu_t = 1/l^*$. Light reflected from a turbid medium has typically entered the object up to a depth z of a (few times the) transport mean free path l^*. A limitation of this technique is that any individual measurement gives an average of the assumed homogenous and generally rather large sample volume; spatially resolved measurements are not possible. In this article we describe a scheme that provides a 2D map of the diffuse scattering properties of a complex, multiple scattering medium by recording a single image with an exposure time in the milisecond range.

#155084 - $15.00 USD Received 20 Sep 2011; revised 24 Nov 2011; accepted 28 Nov 2011; published 20 Dec 2011

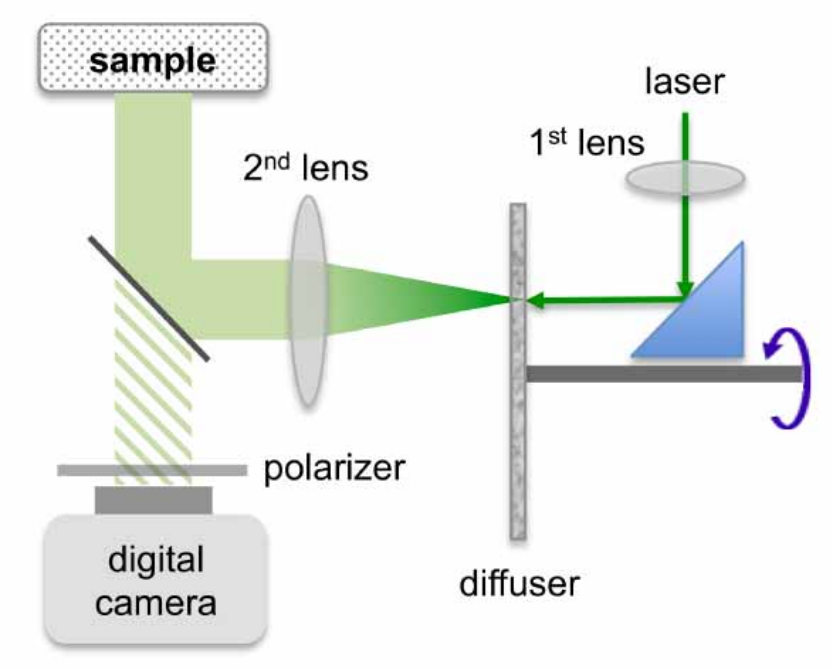

Fig. 1. Experimental setup displaying beam path and all components. A single-mode diode-pumped solid-state laser operating at 532 nm is deflected onto a ground-glass optical diffuser mounted onto a rotating motor. The coherence length of the laser beam being sufficiently large ($l_{coh} \gg l^*$) is critical for the proposed technique. The light scattered from the diffuser is collimated by a lens and directed by a semi-transparent beamsplitter onto the sample. A digital camera images the sample surface through an objective. A crossed polarizer is mounted in front of the camera to attenuate specular reflections.

2. Experimental setup

In general, measurement of diffuse scattering in the reflection geometry is of great interest for many applications including *in-vivo* biological imaging as access to only one side of the sample region is required. In such a context, spatially-resolved measurements are desirable and this is traditionally achieved by placing distinct incident and detector optical fiber probes on the sample surface and separated by a given distance [7]. Light scattered by the sample and measured by the detector is processed using the known separation distance to recover the sample scattering properties. Alternatively, the diffuse broadening of a point source at a sample surface can be imaged and analyzed to extract l^* [1]. While useful and already available in early commercial implementations, all of these methods require scanning of either the probe or the sample to map a sample area. In contrast to these real-space approaches spatially patterned illumination has recently been introduced as a method to map tissue optical properties [12]. This method bears some similarities to our approach although it lacks the high spatial resolution we can achieve in single frame acquisition. Patterned illumination has also been applied to optimze fluorescence optical tomography [13]. The experimental setup is presented in Fig. 1. A collimated laser beam (λ = 532 nm) is slightly focused (or expanded) onto a ground glass diffuser using a first lens. The diffusor is mounted on an electric motor and the light impinges on the diffuser at a distance of about 10 mm from the rotation axis. The size w_0 of the illumination spot on the diffuser can be adjusted by positioning lens (1) at a certain distance relative to

#155084 - $15.00 USD Received 20 Sep 2011; revised 24 Nov 2011; accepted 28 Nov 2011; published 20 Dec 2011

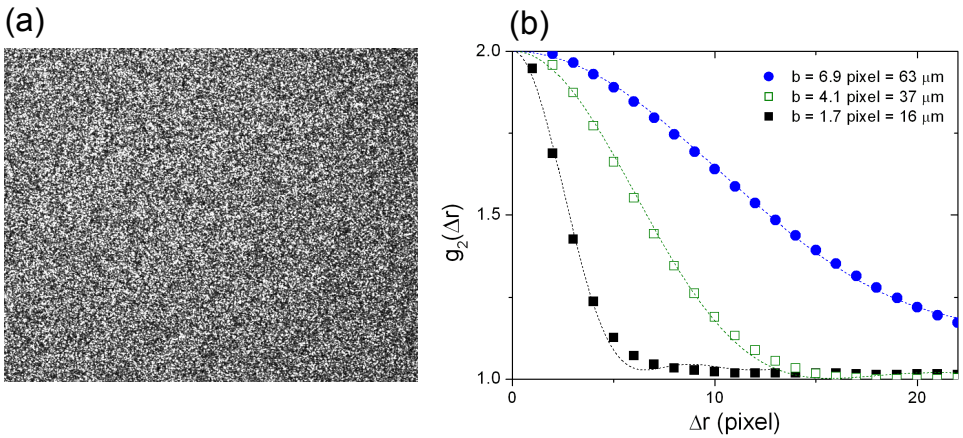

Fig. 2. (a) Direct image of speckle beam taken by placing camera at the sample position for the smallest speckle size considered. (b) Normalized intensity correlation function $g_2(\Delta r)$ obtained by the inverse Fourier transform of the speckle power spectrum. The speckle size is varied from $2b$ = 36 μm to 126 μm.

the diffuser. The forward-scattered light is collimated using a second lens with a focal length L = 4 cm thus creating a homogeneous speckle beam with a width $\approx$ 2 cm [14]. We obtain longitudinally elongated near-field speckles and use them to illuminate the sample placed at a distance of about $6-8$ cm from the lens. In this so-called *deep-Fresnel* regime the speckles have a Gaussian shape with a well defined size $b \approx \pi\lambda L/w_0$ [15]. Thus for a laser beam of diameter 1 mm we expect a speckle size 2b $\approx$ 100 μm. The actual beam-speckle size b is determined by placing the camera at the sample position. From the raw images we can calculate the spatial correlation function and thus b as described in [16] (Fig. 2). The speckle beam obtained in such a way impinges on the sample. A digital camera focused to the sample surface (Prosilica GC 650, Allied Vision Technology, pixel size $a = 7.4\mu$m, 659 $\times$ 493 pixel) records images with 0.83 $\times$ magnification and with its aperture set to produce image speckle roughly of the order of the size of a camera pixel. We use a semi transparent beamsplitter to speparate the illumination and detection path. The motor is then set to rotate at a fixed frequency f and the camera exposure time τ_{exp} is set to average over a large number of different speckle configurations produced by the diffuser (a more detailed discussion concerning the exposure is given later in the text). It should be clarified that image speckle is of a different origin than beam speckle. The latter is induced by the ground-glass diffuser and its purpose is to impose a random field illumination pattern onto the sample that can be quickly varied. Image speckle, on the other hand, arises regardless of any illumination patterning; even with plane wave illumination, interference effects of the diffuse backscattered coherent laser light yield speckle at the image plane. It is this image speckle which is set at approximately the size of the camera pixel.

Such random modulation of the beam-speckle also influences the spatial fluctuations of the diffusely-backscattered image speckle. The proposed method for 2D mapping of l^* using the setup described above can best be explained by studying two limiting cases in which beam speckle size is either much smaller ($b \ll l^*$) or much larger ($b \gg l^*$) than the sample transport mean free path. It can be shown that half of incident photons leave the sample at a distance of less than $\sim 3l^*$ from the point of entry while the other half leaves at greater distances [17, 18]. Thus, in the case where $b \ll l^*$, the diffusely backscattered electric field amplitude at any point on the imaged surface is composed of contributions from many incident beam-speckles origi-

#155084 - $15.00 USD Received 20 Sep 2011; revised 24 Nov 2011; accepted 28 Nov 2011; published 20 Dec 2011

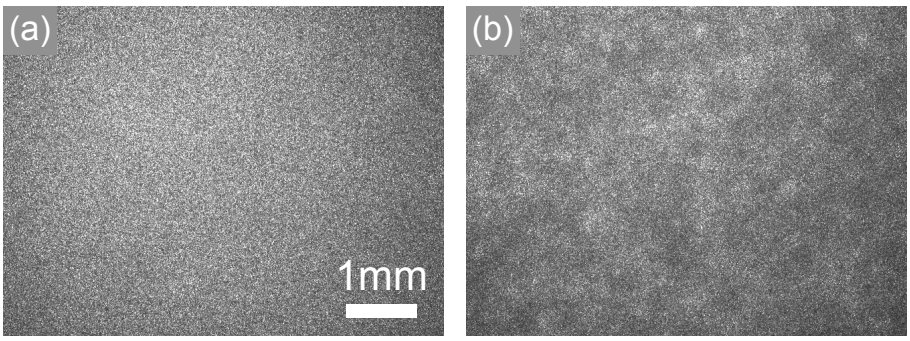

Fig. 3. Recorded image speckle with motor at rest for a sample with l^* = 245 μm (a) and l^* = 50 μm (b). The size of the incident beam-speckle is $2b = 3.4$ pixel (32 μm). A random pattern (defined by the incident beam speckle) superimposed on the fine image speckle is apparent in (b) but not (a).

nating from a surface area $\sim 10\pi l^{*2} \gg b^2$. Rotating the ground glass alters the configuration of the speckle beam randomly and therefore also leads to random fluctuations of the image speckle. By choosing a sufficiently long camera exposure, random temporal fluctuations of the image-speckle arising from fluctuations of the speckle beam are time-integrated. This then results in a spatially homogeneous intensity distribution that is measured by the camera. In the opposite limit $b \gg l^*$, the scattered field amplitude at a given point on the imaged surface is composed of contributions of only a single incident beam-speckle within the typical surface area $\sim 10\pi l^{*2} \ll b^2$. If the field amplitude of the beam-speckle is varied this does not alter the local statistical properties (such as the variance) of image speckle. For a given pixel on the imaging detector (being matched to the image speckle size), this case is similar to just turning the laser light on and off; since the sample properties are time-invariant the local spatial variance of the time-integrated image speckle remains unchanged. The transition between these two limiting cases is continuous and therefore the signature of the residual image speckle can be used to map l^* values.

3. Experimental verification

3.1. Homogeneous samples - calibration curve

In order to demonstrate the proposed l^* imaging method, both homogenous and spatially heterogeneous samples were studied. In the experiments presented here we only use sufficiently solid samples and therefore intrinsic speckle fluctuations due to Brownian motion of scattering centers can be neglected. In the first experiment we have prepared four samples with different values of l^* by mixing a suspension of 990nm diameter polystyrene spheres with water and gelatin (final gelatin concentration 4%, 2% in one case). After one day the samples were solid as verified using DWS (DWS Rheolab, LSInstruments, Switzerland) [5, 9]. The four different concentrations of polystyrene particles doped into the gelatin (by weight) are 1.25 % ($l^* = 245\mu$m), 2.08 % ($l^* = 147\mu$m), 4.15 % ($l^* = 74\mu$m), 6.20 % ($l^* = 50\mu$m, gelatine 2% - solid). The values for l^* have been calculated analytically assuming a particle and solvent refractive index of $n_p = 1.59$, $n_s \simeq 1.34$) [19].

By visually comparing speckle images from two samples (one with a short l^* and one with a large l^*, diffuser at rest), one can easily observe the phenomena discussed previously as shown in Fig. 3. A random pattern (defined by the incident beam speckle) superimposed on the fine image speckle is apparent in Fig. 3(b), but not Fig. 3(a). A detailed analysis of this effect

#155084 - $15.00 USD Received 20 Sep 2011; revised 24 Nov 2011; accepted 28 Nov 2011; published 20 Dec 2011

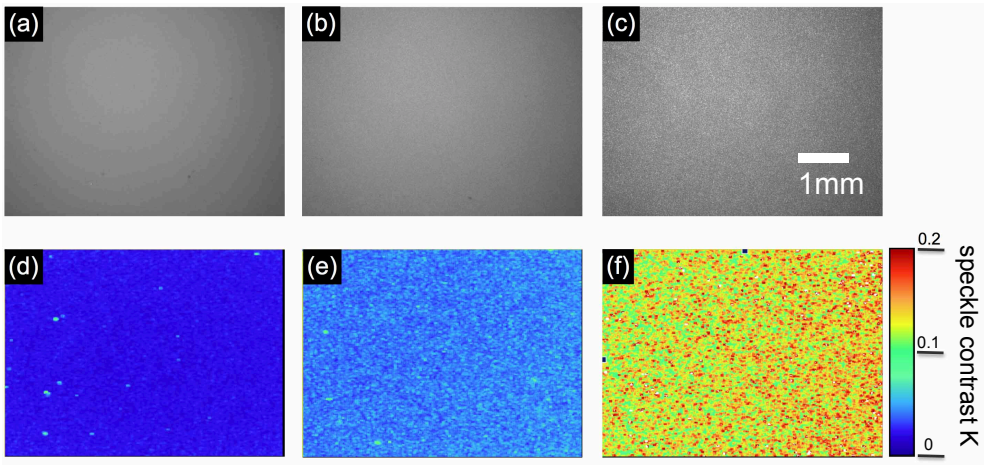

Fig. 4. (a)–(c) Recorded speckle images of gelatin with polystyrene beads with motor spinning at 50Hz (exposure time 30 ms) with characteristic parameters b/l^*= 0.065, 0.32, 1.3, respectively. (d)-(f) Processed maps of local image speckle contrast with average contrast increasing from 1.9%, 3.9% to 12.4 %, respectively.

allows one to extract an estimate of l^* for a given sample. Such an approach would rely on the same principles as the structured illumination method discussed in reference [12]. However, the spatial resolution of that method is limited since the illuminating speckle must be on the order of l^* or larger to produce a measurable effect.

It should be emphasized that the method presented here provides a much higher intrinsic resolution. This is made possible by analyzing the properties of the residual image speckle as the pattern of the illumination field is rapidly varied. Figure 4 illustrates how the resulting image speckle (diffuser in motion at 50 Hz) evolves as a function of l^*, where l^* decreases from Figs. 4(a) to 4(b) and further to Fig. 4(c). Figures 4(d)–4(f) give the associated maps of the local speckle contrast K (standard deviation / mean) calculated for each pixel position over the surrounding 25-pixel area. It is shown that a shorter l^* leads directly to an increase of the average measured local variance.

To confirm the trend and demonstrate that the measured contrast is in fact a function of l^* normalized to the beam speckle size b, a further study of the polystyrene in gelatin samples was performed for varied beam speckle sizes. Figure 5 summarizes the results and confirms the quantitative relationship of K with the normalized reduced scattering coefficient $b \cdot \mu_t = b/l^*$ and reveals that the image speckle contrast increases linearly for small and intermediate values $b/l^* \leq 1$. For higher values it must saturate since it cannot exceed the speckle contrast for plane wave illumination, in the present case 0.295. Overall the data can be described empirically by a *tanh*-fit. With a single setting of the incident speckle-beam forming optics, it is possible to cover roughly the range b/l^*=0.05 - 5, corresponding to two orders of magnitude in μ_t. For example with $b = 50\mu$m one can probe scattering coefficients roughly from μ_t = 1 mm^{-1} [l^* = 1 mm] to 100 mm^{-1} [l^* = 10 μm].

3.2. High resolution imaging

While the previous experiments exploited only an average of the local measured image contrast for a homogenous sample, it is possible to measure and image local scattering properties with high resolution. Figure 6 shows a contrast map [20] of white paper ($l^* \simeq 11 \pm 1$ μm), the right side of which is covered with correction tape ($l^* \approx$1-2 μm) with part of the correction

#155084 - $15.00 USD Received 20 Sep 2011; revised 24 Nov 2011; accepted 28 Nov 2011; published 20 Dec 2011

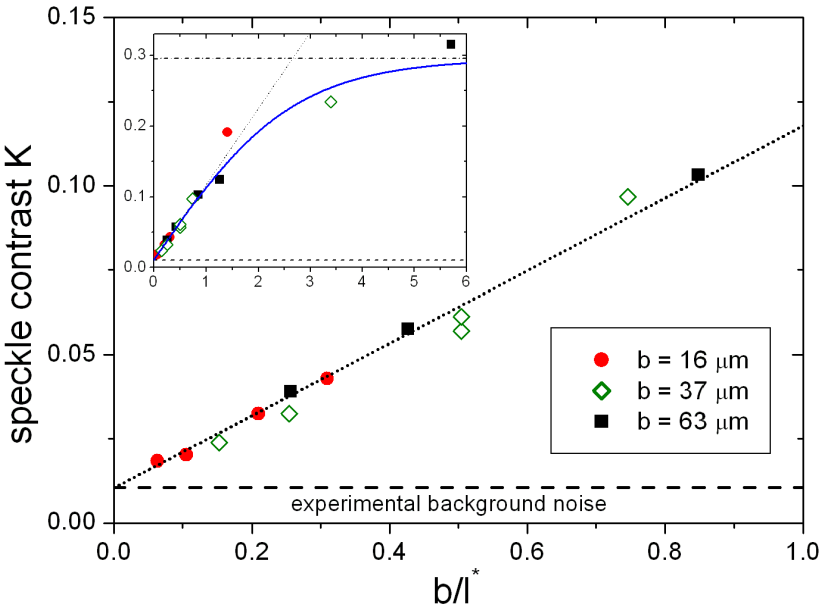

Fig. 5. Speckle contrast K of image speckle as a function of b/l^* (symbols). Data for three different speckle beam settings (b) is shown. The transport mean free path is l^* = 245, 147, 74, 50 μm for the polystyrene in gelatin samples and $l^* \simeq 11\mu$m for white paper. Motor spinning at 50Hz and camera acquisition set to $\tau_{exp} = 30$ ms exposure. Solid line (inset) : An empirical *tanh*-fit provides a quantitative link between the measured contrast and sample scattering properties ($K = 0.285 \cdot \tanh[0.38 \cdot b/l^*] + 0.01$). For $b/l^* < 1$ the speckle contrast scales linearly (dotted lines). For $b/l^* \gg 1$ the speckle contrast for plane-wave illumination, $K = 0.295$, is recovered (dashed-dotted horizontal line).

tape removed (single scratch). The spatially averaged l^* of paper and correction tape were determined using DWS. The scattering properties of the two materials are well-differentiated and the structure of the sample is well resolved. The local l^* can be extracted from the speckle contrast image via the empirical *tanh* fit.

3.3. Minimum exposure time and applications to samples with internal motion

The product of camera exposure time τ_{exp} and ground-glass rotation frequency f dictates (for a solid sample) the number of beam-speckle configurations over which the image represents an average. By varying the motor speed and observing the variance of the resulting beam-speckle images taken at the sample position (as shown in Fig. 7) we can give an estimate for the value $\tau_{exp} f$ required for a decent average. In our experiment, sufficient averaging is observed for the product $\tau_{exp} f > 0.05$. For a maximum value of $f = 200$ Hz in our case this corresponds to a lower limit for the exposure time of $\tau_{exp} \sim 250$ μs. Using a high-speed brushless DC electric motor at $f \sim 1000$ Hz and illuminating the ground-glass at a larger radial distance from the rotation axis, exposure times on the microsecond scale could be realized. Such a high-speed version of our experiment would also be suitable for the study of liquid samples since the typical time scale for speckle fluctuations of multiply scattered light is on the order of 100 μs or more in the reflection geometry [9]. Microsecond acquisition times will however additionally demand a fast and sensitive camera as well as sufficient laser power.

#155084 - $15.00 USD Received 20 Sep 2011; revised 24 Nov 2011; accepted 28 Nov 2011; published 20 Dec 2011

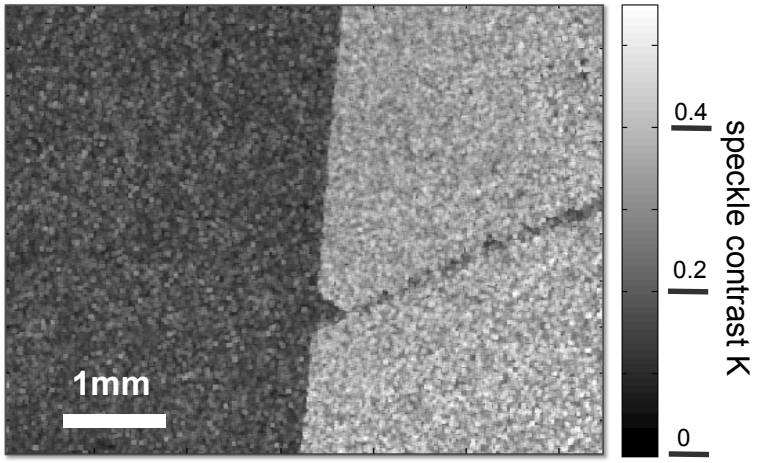

Fig. 6. High resolution greyscale coded map of speckle contrast K for white paper (left) covered with a correction tape (right) that is scratched once with a knife. Motor spinning at 50 Hz, 230 ms exposure, beam speckle size $b = 16\mu$m, 5×5 -pixels used for local contrast analysis [20]. Sample also shows a slight intensity contrast - not shown - due to the finite reflectivity of the correction tape. The local l^* can be extracted from the speckle contrast image via the empirical *tanh* fit, Fig. 5.

4. Summary and conclusions

In summary we have presented a simple scheme to map the diffuse scattering properties of a turbid medium. We have demonstrated its feasibility and established and verified the main principles. Namely we have shown that we can use the post-averaging residual speckle contrast to construct a map of the reduced scattering coefficient μ_t. A linear relationship between the speckle contrast and the value of l^* has been found. This value of l^* is representative of the local superficial scattering properties of the medium, wherein the contributions to this local average are dominated by the material at the surface and decay strongly in the vertical direction. This effect as well as the ability of the technique to resolve sub-surface inhomogeneities has been characterized previously [21].

The advantages or our approach are its simplicity and consequently low cost, high resolution and extremely short acquisition time. While currently limited to solid samples, an extension of the method to liquid media is straightforward though technically more demanding and thus more costly. A further limitation of the method is that it does not provide information about the sample absorption coefficient μ_a [6]. However, the latter could be included via an analysis of the reflected intensity at least for the case of weak absorption where $\mu_a \ll \mu_t$. Since we are working with time-averages and a broad statistically distributed speckle beam, an extension to diffuse 3D tomography is precluded. Equally the method cannot be applied to diffuse imaging of fluorescence due to the absence of interference speckle. Coherence requirements also complicate the measurement of spectral properties. Limited spectroscopic information could be obtained by using a set of two or three lasers and a color digital camera. It would also be feasible to use a supercontinuum source along with a set of filters to extract both scattering and spectroscopic properties in a similar fashion as has been implemented for transmission speckle contrast [22] and coherent backscattering measurements [23].

Although most previous methods of this kind have been targeted to biomedical imaging we think the present method might be particularly suited for studies of soft materials for applica-

#155084 - $15.00 USD Received 20 Sep 2011; revised 24 Nov 2011; accepted 28 Nov 2011; published 20 Dec 2011

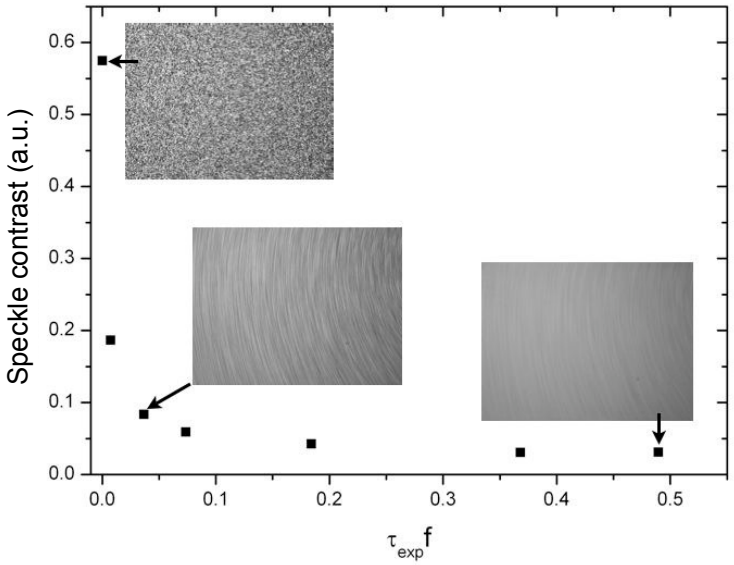

Fig. 7. Speckle contrast of beam-speckle imaged for varying combinations of camera exposure time (τ_{exp})and ground-glass diffuser rotation frequency (f). Images are shown for three data points, demonstrating the averaging effect at larger exposure-time/rotation-frequency combinations.

tions such as phase separation, sedimentation or creaming of highly turbid suspensions, slurries or emulsions. It might also be applicable to dental imaging [24] or studies of bone tissue and related questions. An interesting outlook would be to combine the method with laser speckle imaging [25]. Keeping the diffuser at rest would allow one to study dynamic properties of the medium while spinning the ground glass would provide access to diffuse scattering properties in a single experimental configuration.

Acknowledgments

We would like to gratefully acknowledge financial support from the CTI (Innovation promotion agency of the Swiss Confederation) under grant 9884.1. We thank Axelle Amon for insightful discussions and Frédéric Cardinaux for help with the data treatment.

#155084 - $15.00 USD Received 20 Sep 2011; revised 24 Nov 2011; accepted 28 Nov 2011; published 20 Dec 2011